Phase transition lowering in dynamically compressed silicon

Mcbride, E. E.; Krygier, A.; Ehnes, A.; Galtier, E.; Harmand, M.; Konôpková, Z.; Lee, H. J.; Liermann, H.-P.; Nagler, B.; Pelka, A.; Rödel, M.; Schropp, A.; Smith, R. F.; Spindloe, C.; Swift, D.; Tavella, F.; Toleikis, S.; Tschentscher, T.; Wark, J. S.; Higginbotham, A.;

Originally published:

September 2018

Nature Physics 15(2019), 1745-2481

DOI: https://doi.org/10.1038/s41567-018-0290-x

Phase Transition Lowering in Dynamically-Compressed Silicon

E. E. McBride[1,*,†], A. Krygier[2], A. Ehnes[1], E. Galtier[3], M. Harmand[2], Z. Konôpková[1], H. J. Lee[3], H.-P. Liermann[1], B. Nagler[3], A. Pelka[4], M. Rödel[4], A. Schropp[1], R. F. Smith[5], C. Spindloe[6], D. Swift[5], F. Tavella[3], S. Toleikis[1], T. Tschentscher[7], J. S. Wark[8], and A. Higginbotham[9]

[1] *Photon Science, Deutsches Elektronen-Synchrotron DESY, Notkestrasse 85, D-22607, Hamburg, Germany*

[2] *IMPMC, UPMC, MNHN, IRD, Paris, France*

[3] *SLAC National Accelerator Laboratory, 2575 Sand Hill Road, Menlo Park, California 94025, USA*

[4] *Helmholtz-Zentrum Dresden-Rossendorf, P.O. Box 510119, D-01314 Dresden, Germany*

[5] *Lawrence Livermore National Laboratory, 7000 East Avenue, Livermore, California 94550, USA*

[6] *Central Laser Facility, STFC, Rutherford Appleton Laboratory, Harwell Oxford, Didcot, OX11 0QX, United Kingdom*

[7] *European XFEL GmbH, Holzkoppel 4, D-22869 Schenefeld, Germany*

[8] *Department of Physics, Clarendon Laboratory, University of Oxford, Parks Road, Oxford OX1 3PU, UK*

[9] *York Plasma Institute, Department of Physics, University of York, York, YO10 5DD, UK*

[*] *emcbride@slac.stanford.edu*

[†] *Present address: SLAC National Accelerator Laboratory, 2575 Sand Hill Road, Menlo Park, California 94025, USA and*

[‡] *European XFEL GmbH, Albert-Einstein-Ring 19, D-22761 Hamburg, Germany*

Silicon, being one of the most abundant elements in nature, attracts wide-ranging scientific and technological interest. Specifically, in its elemental form, crystals of remarkable purity can be produced. One may assume that this would lead to Si being well understood, and indeed, this is the case for many ambient properties, as well as for higher pressure behaviour under quasi-static loading. However, despite many decades of study, a detailed understanding of the response of silicon to rapid compression such as that experienced under shock impact – remains elusive. Here, we combine a novel Free Electron Laser (FEL) based X-ray diffraction geometry with laser-driven compression to elucidate the importance of shear generated during shock compression on the occurrence of phase transitions. We observe the lowering of the hydrostatic phase boundary in elemental silicon, an ideal model system for investigating high-strength materials, analogous to planetary constituents. Moreover, we unambiguously determine the onset of melting above 14 GPa, previously ascribed to a solid-solid phase transition, undetectable in the now conventional shocked diffraction geometry; transitions to the liquid state are expected to be ubiquitous in all systems at sufficiently high pressures and temperatures.

Since Bancroft[1] first reported shock-induced polymorphism over fifty years ago, solid-solid and solid-liquid phase transitions have been the focus of innumerable shock-compression studies. Velocimetry techniques have been key diagnostic tools in the inference of such phase transitions, with plateaus in density interpreted as plastic deformation or phase transitions. However, such methods are not able to shed light on the crystallographic phase of material, especially since effects, such as kinetics, have the potential to cause significant differences between statically and dynamically determined sample response. In this work we focus on the behaviour of elemental silicon (Si), which despite being well-understood under hydrostatic conditions, remains a subject of vigorous debate following dynamic loading[2–6]. Under uniaxial compression conditions, significant shear is generated as the material resists compression, a direct consequence of the material strength, yet the nature of the shear-relieving mechanism plasticity or via a phase transformation), and the structure(s) of the proposed high pressure phases remain largely unknown.

More generally, previous works suggest that phase boundaries in rapidly-compressed solids depend strongly on the strain-rate of the compression, with a higher strain-rate drive (i.e. shock compression) leading to a higher transition pressure[7, 8]. However, it is also suggested that the anisotropic nature of planar shock compression may lead to significant shear stresses in samples, which can lead to lowering of phase transition boundaries from hydrostatically determined values[9]. This points to the danger in the typical method of assigning phase transitions under shock loading to those observed under hydrostatic conditions at similar pressure conditions. Moreover, it means that phase transition pressures determined from dynamic compression experiments must be interpreted with care before application to hydrostatic systems, such as planetary interiors.

As one of the most abundant elements in nature, Si attracts wide-ranging scientific and technological interest, and hence many of its properties at ambient conditions, and at higher pressure under quasi-static loading, are well understood. Static compression experiments reveal a complex phase diagram, where thirteen different polymorphs have been observed to date[10–17]. Of particular relevance to this work is the highly reconstructive phase transformation from the ambient pressure semi-conducting cubic diamond (CD) structure to the metallic β-tin structure at $\sim$12 GPa, with an associated 20% volume collapse[10]. On further increase of pressure, the closely related orthorhombic phase *Imma* is formed, which in turn transforms to a simple hexagonal (SH) crystal structure at 16 GPa[11, 13].

However, among dynamic-loading experiments, a clear consensus in the data is yet to emerge. Such studies using velocimitery measurements report the observation of three distinct waves traversing the sample[3–6]. For example, early work by Gust & Royce find waves at 5.4 GPa, 10.1 GPa and 13.7 GPa for compression along the [111] crystal direction. Such waves are often interpreted as occurring at the onset pressure of shear dissipation mechanisms, such as plasticity i.e. by the generation and motion of defects, or via a phase transformation. These velocimetry data are therefore often taken to suggest that the first phase transition occurs at 10 GPa, in broad agreement with the hydrostatically determined value of 12 GPa. The second wave emerging at 5.4 GPa is then assigned to plasticity within the compressed CD phase. However, positive identification of the mechanisms associated with these waves in silicon is still outstanding.

Numerous laser-driven compression experiments coupled with traditional laser-plasma X-ray sources have failed to find evidence for higher pressure phases in compressed single crystal samples. Molecular dynamics (MD) simulations have suggested that this may be due to any new phases forming small (sub-micron), potentially misaligned grains, which would lead to highly diffuse diffraction features, difficult to detect in experiments using these conventional laser-plasma X-ray sources[18]. The structure of the high pressure phase(s) adopted by Si on the Hugoniot, and the nature of the two waves which emerge following the elastic wave, remains unknown, leaving the dynamic behaviour of Si a matter of ongoing debate.

Here, we present a systematic study of the behaviour of Si following laser-driven shock-compression. Specifically, we employ polycrystalline Si samples, and exploit the high brightness X-rays offered by Free Electron Lasers to study diffuse reciprocal space features. In doing so, we are able to identify the structural response of the sample from its ambient CD phase, through to shock-induced melting at 14 GPa, coinciding with the emergence of the third wave.

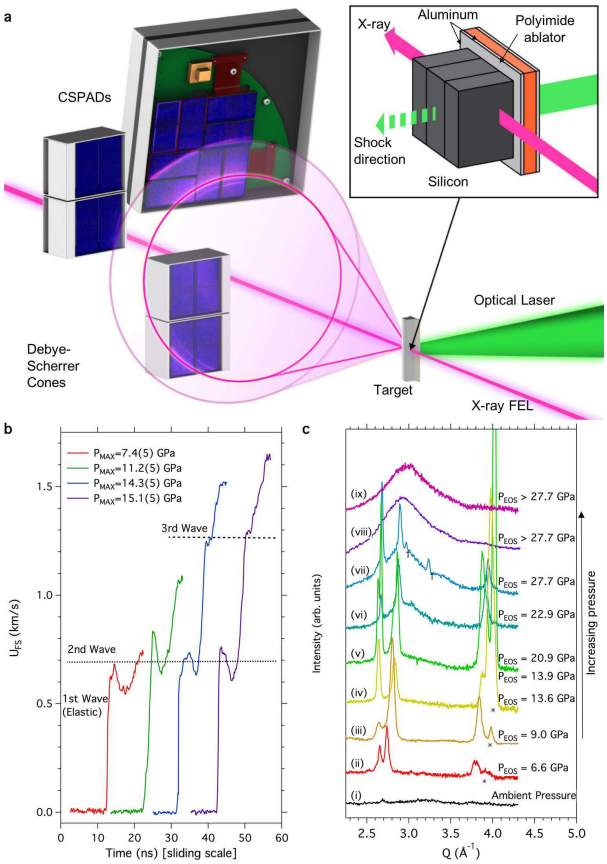

FIG. 1. **Experimental configuration and data examples: a** the transverse configuration whereby the compression laser was perpendicular to the X-ray beam. **b** Velocimetry data (VISAR) lineouts showing free surface velocity (U_{FS}). Laser intensity increases to the right. Dashed lines indicate the onset of the 2nd and 3rd wave. **c** Azimuthally integrated 1D diffraction patterns as a function of increasing laser intensity and hence increasing pressure in both the transverse: (i), (ii), (iv), (v), (ix) and collinear (iii), (vi), (vii), (viii) configurations. Peaks marked with the ∗ symbol belong to the compressed cubic diamond phase. Peaks marked with the † symbol cannot be described by the cubic diamond, β-tin, *Imma*, or simple hexagonal phases.

Crucially, we observe a lowering of two solid-solid phase boundaries from their hydrostatically determined values, suggesting the significant role that shear stress plays in modifying the phase diagram of Si.

Experiments were conducted at the Matter in Extreme Conditions (MEC) endstation at the Linear Coherent Light Source (LCLS)[19]. Polycrystalline silicon samples, with 50 μm polyimide ablators, were shock compressed via irradiation with the nanosecond pulsed Nd:glass laser system. During shock transit through the Si sample, the high brightness LCLS X-ray beam was used to determine the structure of the material via X-ray diffraction in a Debye-Scherrer geometry. Two distinct experimental geometries were employed in this work. The first is a 'collinear' geometry, where the X-ray beam is incident at around 11° to the target normal, and thus to the direction of shock compression. This is a common geometry at LCLS[20–24], and other laser-plasma based experiments[25–28]. It is described in Supp. Info. Sec. I.

However, this configuration has the distinct disadvantage of providing a signal that integrates through all states within the sample. This greatly complicates both the detection and the analysis of low-symmetry complex phases on the Hugoniot, including melting, where multiple high-pressure phases may be present in successive compression waves. The second 'transverse' geometry aims to resolve this shortcoming by driving the shockwave *perpendicular* to the LCLS beam direction (Fig. 1 (a)). In this configuration, by taking advantage of the highly collimated and microfocussed beam available at the LCLS we ensure that, predominantly, a single wave in the multi-wave compression response is probed, greatly aiding interpretation and phase identification. Further details of the experimental configurations and target designs employed are confined to the Methods section and Supp. Info. Secs. I-III. A detailed comparison of the collinear and transverse configurations is found in the Supp. Info. Sec. VI.

Utilising optical velocimetry (VISAR) combined with X-ray diffraction in the collinear configuration, the wave profile as a function of laser intensity was investigated, and the sample pressure was inferred from the free surface

velocity, U_{FS} (Supp. Info. Sec. IV). An example of typical velocimetry traces may be seen in Fig. 1 (b). The wave profiles observed were in good agreement with previous laser and gas-gun based shock experiments[3, 6]. Here, consistent with previous studies, we observe the significant elastic response, followed by a pullback and a second wave, often ascribed to plastic deformation. Above 14 GPa (U_{FS} ∼1.3 km/s), we observe a plateau in the velocity-time data indicating a change in sound speed in the sample. Following the plateau we observe the emergence of a third wave, again consistent with previous studies. The plateau is described as the onset of a structural phase transition. As these polycrystalline samples have large grains (∼100 μm) with different orientations, we observe that the magnitude of the elastic response differs from shot to shot depending on the starting orientation of the sample – varying from 6.6(5) GPa to 7.9(5) GPa (Supp. Info. Fig. 6). This is consistent with the previously-reported orientational dependence of the elastic response of single-crystal[4]. We also note that the plateau observed is *independent* of the starting orientation, consistent with previous studies[6].

Figure 1 (c) shows azimuthally integrated 1D diffraction patterns as a function of increasing laser intensity, and hence increasing pressure, in both geometries (see caption). As the initial grain size of the sample is large compared to the X-ray beam diameter (10-40 μm), prior to the shock, we are unlikely to satisfy the Bragg condition due to preferred orientation. Therefore the diffraction profile is flat (Fig. 1 (c i)). As laser intensity is increased we observe the emergence of sharp peaks, consistent with the formation of a new phase (Fig. 1 (c ii)). Note, in some diffraction patterns we also observe reflections belonging to the compressed CD phase ($*$ symbols), suggesting the generation of smaller grains of CD material between domains of the newly formed high pressure phase. An example of the 2D diffraction images may be seen in Fig. 1 (a), and in Supp. Info. Fig. 7. Here, the smooth Debye-Scherrer rings belong to the high pressure phase, and indicate that the large grains of the initial CD phase have broken up into nanometer-sized grains, inferred from the smooth powder rings observed in the 2D diffraction patterns.

In the collinear configuration, at a pressure of 7.4(5) GPa, just above the elastic limit, we observe an increase in scattering intensity of diffraction features at Q ∼ 2.7 and Q ∼ 3.8 Å^{-1} (Fig. 2 (ii)), but here the structure cannot be fully resolved. By using the same laser-drive conditions, in the transverse geometry we can clearly assign these features to the β-tin structure, with a c/a ratio of 0.550, as shown by the diffraction pattern Fig. 2 (iii). A Le Bail fit is shown by the dotted black line, and is in excellent agreement with the data [29]. A distinguishing feature used to identify the high pressure phases is the evolution of the c/a ratio as a function of pressure. The β-tin structure has a c/a value of 0.550, and the SH a value of 0.533; the c/a ratio of the *Imma* structure evolves from 0.550 to 0.533 with increasing pressure [12] (See Methods). As laser intensity, and hence pressure is increased to 9.0(5) GPa, we observe what can be best described as a mixed phase (Fig. 1 (c iii)), consisting of both the β-tin and *Imma* structures. At 9.4(5) GPa, the high-pressure phase transforms completely to the *Imma* structure (Fig. 1 (c iv), with no evidence of co-existence with β-tin. The *Imma* structure also co-exists with the compressed CD phase. This phase co-existence has previously been observed in quasi-hydrostatic diamond anvil cell studies [12, 13].

Hence, we observe that, for laser-driven compression, rather than through plastic deformation, the significant shear stress at the Hugoniot elastic limit (HEL) is consistent with being relieved via a phase transformation to a mixed phase of CD and a high-pressure structure i.e. the dominant shear dissipation mechanism as the material is compressed beyond the HEL is a phase transformation. As suggested by Mogni *et al.*[18] in their MD simulations, we observe that the second wave is concurrent with transformation to a body-centred tetragonal structure, yet we identify it as the β-tin phase, rather than *Imma* as they suggest. Moreover, we note a considerable lowering of the onset of the β-tin phase transformation as compared with hydrostatic diamond anvil cell experiments – from 12 GPa in ref. [12] down to as low as 5.4(5) GPa in this work. Such an effect has been observed in *ab initio* simulations where it was suggested that the transition pressure decreases from 11.4 GPa under hydrostatic conditions to 3.9 GPa under uniaxial compression[30]. Additionally, in experimental studies combining resistivity measurements with nanoindentation techniques, Gupta & Ruoff[31] note that the onset of the metallic phase, interpreted as the onset of the β-tin phase, lowers from 12 GPa in under static loading, to 8 GPa under a compression rate of 1 kbar/sec, for compression along the [100] axis. This work, therefore, highlights the failure of the long-standing approach of understanding the nature of shock-induced phase transformation through comparison with hydrostatic phase transformations occurring at similar pressures.

As the *Imma* structure is further compressed, we observe an evolution of the c/a ratio as a function of normalised volume (V/V_0), (Fig. 3 (a)) away from the ideal experimental and theoretical β-tin values (0.550 and 0.549) towards the ideal SH values (0.535 and 0.533), with the same trend observed in both the collinear and transverse experimental configurations[12, 32]. At a c/a ratio of 0.537, and a corresponding V/V_0 of 0.681, we note a distinct change in the gradient of the c/a ratio, indicating a change in compressibility of the structure. This change occurs at a pressure inferred via VISAR of 13.8(5) GPa, coinciding with the emergence of the third wave discussed above. One should note that in our data obtained in the collinear configuration, we do not observe any additional scattering in the diffraction patterns, that would be indicative of the formation of a second new phase, and hence account for such a change in compressibility (Fig. 3 (b)).

Owing to the unique ability that we are afforded by the transverse configuration, we are able to isolate each of the different waves as they traverse the sample following shock compression. We are therefore able to determine that the

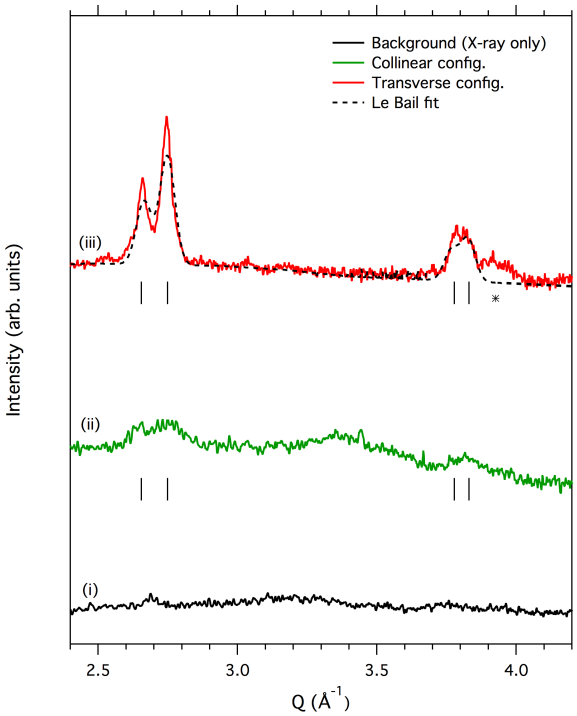

FIG. 2. **The greater sensitivity of the transverse configuration** 1D diffraction profiles in the collinear (ii) and transverse (iii) configurations. Profile (i) shows X-ray only pre-shot. The dotted black line under profile (iii) is a Le Bail fit to the β-tin structure. The tick marks underneath diffraction profiles (ii) and (iii) indicate the position of the first four β-tin reflections. The $*$ symbol indicates reflections belonging to the compressed cubic diamond phase.

change in c/a ratio coincides with the emergence of a broad diffuse feature, characteristic of a liquid or amorphous sample, in coexistence with the solid (Fig 3 (b) and Fig. 1 (c v)). Moreover, we note that both the shape and position of the broad diffuse peak are in good agreement with that of liquid silicon at 14 GPa (Fig. 3 (c)), as determined through static compression techniques combined with synchrotron X-ray diffraction[33]. Notably, we do not observe the second strong broad diffraction peak at Q$\sim$3.6 Å^{-1} characteristic of the high-density amorphous polymorph at P$\sim$13 GPa, and therefore conclude that the diffuse scattering is most consistent with the liquid state (Supp. Info. Fig. 9).[34] The third wave, rather than being due to a solid-solid phase transition as previously reported, is therefore attributed to shock-induced melting along the Hugoniot.

In comparing diffraction from both configurations, we note that in the collinear configuration we are overwhelmed by the solid Bragg diffraction and insensitive to the presence of liquid diffraction until we have incubated a significant fraction of the liquid phase (Supp. Info. Fig. 13). Moreover, in the collinear configuration, the amount of volumetric compression as determined from the diffraction patterns is directly related to the timing of the X-rays with respect to the supported shock (Supp. Info Fig. 12). It is clear from Fig. 3 (b) that, in the collinear geometry, depending on the timing of the X-rays, we are sensitive to different parts of the wave profile, i.e. to different volumes (and hence pressures), and insensitive to the onset of melting on the Hugoniot.

As pressure is increased, the solid *Imma* phase transforms to the SH phase, and the diffuse feature grows more intense, as a larger volume fraction of the sample is now in the liquid state (Fig. 1 (c vi)). Due to the significant latent heat of fusion of Si, the second highest of the elements, we observe that the Hugoniot follows the melting curve over a considerable pressure range, as indicated by solid-liquid co-existence up to at least a V/V$_0$ of 0.632 (P$\sim$ 27 GPa) as shown in Fig. 1 (c vii). Above 27 GPa, the sample is able to overcome the latent heat of fusion and melts entirely (Fig. 1 (c viii & ix). Such a plateau of the Hugoniot along the melting line, and two-phase coexistence, has been previously reported in laser-driven shock compression studies of diamond[35]. In contrast to recent shock-recovery and MD studies on Si, at similar maximum pressures of 30 GPa, which suggest the formation of localised amorphous banding[36, 37], we observe the occurrence of bulk, or complete, melting of the sample. Hence, we conclude that the formation of bands of amorphous and CD Si is formed on release to ambient pressure following shock compression, demonstrating the importance of *in situ* measurements.

In their recent work combining a gas-gun pressure driver and synchrotron X-ray diffraction, Turneaure *et al.* [38] report that at P$\sim$19 GPa, above the onset of the third wave, Si adopts the SH structure. However, unlike our work,

they find no evidence of melting in their diffraction data. In their study, the sample was initially shock-compressed to a peak pressure of 26 GPa, and only conclusively identified transforming to the SH structure after at least one reflection of the phase transformation wave had passed back through the silicon, releasing pressure. Hence they were probing an off-Hugoniot, and rather complex, hydrodynamic state.

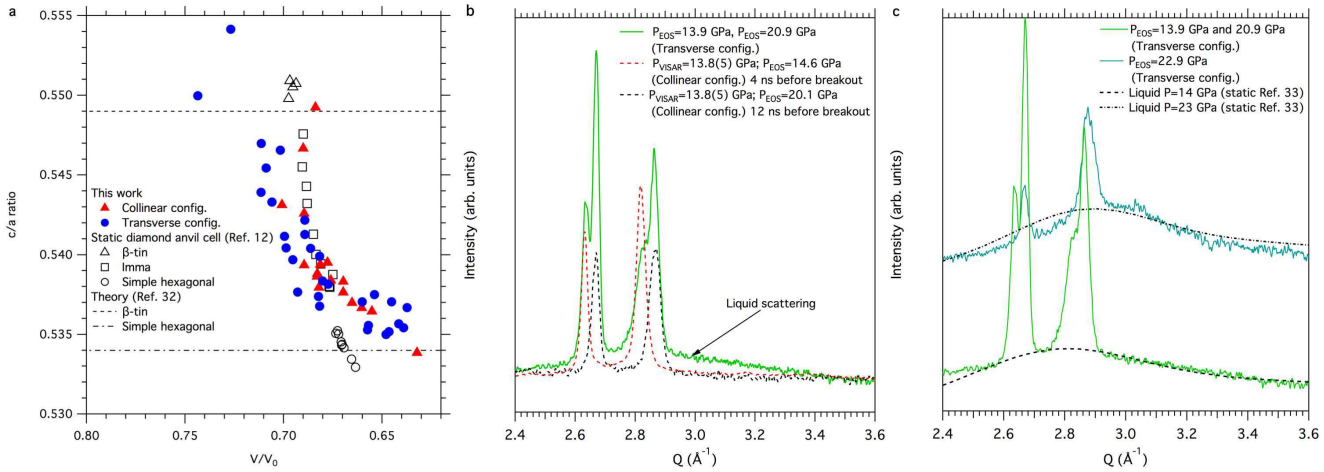

FIG. 3. **Evidence of the onset of melting: a** Evolution of the c/a ratio as a function of volumetric change (V/V_0) in the collinear (blue circles) and transverse (red triangles) configurations. Open symbols are from a hydrostatic diamond anvil cell study Ref. 12: β-tin (triangles), *Imma* (squares), simple hexagonal (circles). Theoretical ideal c/a ratios from Ref. 32 are shown for β-tin (dashed line) and the simple hexagonal (dot-dashed line). **b** Comparison of azimuthally integrated 1D diffraction patterns in the collinear and transverse configurations. In the transverse configuration we are more sensitive to the onset of melting, as indicated by the emergence of a broad diffuse peak characteristic of a liquid phase. **c** 1D diffraction patterns in the transverse configuration showing a significant region of solid-liquid co-existence on the Hugoniot. The emergence of the broad diffuse peak at ∼14 GPa is in good agreement with both the position and shape of the liquid peak as determined by static compression experiments, Ref. 33.

Moreover, the lack of liquid signal in their diffraction data is likely due to the transmission (collinear configuration) geometry employed in their experiment. As we have demonstrated, in the oft used collinear geometry one is unable to resolve the various components of a complex, multi-wave shock structure, and specifically one is insensitive to the incubation of melting along the Hugoniot, particularly where there are regions of solid-liquid coexistence. By using the novel transverse approach, collecting diffraction patterns perpendicular to the shock propagation direction, we have much greater sensitivity to the onset of low-symmetry phase transitions and melting along the Hugoniot, expected in all systems at sufficiently high pressures and temperatures.

The stress-volume plot shown in Fig. 4 compares the relative volume (V/V_0) of the high-pressure phases from this work with recent density functional theory calculations[39], and with static diamond anvil cell work.[12] We clearly observe the occurrence of a shear-relieving solid-solid transition concurrent with the HEL, and the observation of the high-pressure phases at considerably lower pressures than previously reported, below the stability field of the static phases. It should also be noted that the additional reflections marked with the † symbol in diffraction profiles Fig. 1 (c vii) cannot be accounted for by any of the candidate structures observed statically up to 30 GPa – the CD, β-tin, *Imma* or SH structure described in this manuscript. These diffraction peaks suggest that prior to melting entirely, we may reach a mixed phase region between the liquid, the SH phase, and an additional solid phase. A likely candidate is the *Cmca* structure, which has been reported to co-exist with the SH phase at room temperature at close to 30 GPa[15]. However, with the observation of only a few weak reflections it is impossible to provide a full structural solution to conclusively determine from which structure these additional peaks arise.

In conclusion, we have determined the nature of the multiple waves that traverse silicon samples following shock compression. We show that the second wave is concurrent with a phase transition to a β-tin structure, rather than due to plasticity. We further determine that the third wave observed above P∼14 GPa is due to the onset of melting along the Hugoniot, rather than due to a solid-solid transition as was previously reported. We observe that the solid and liquid co-exist over a significant pressure range of ΔP∼10 GPa, before enough energy is supplied to overcome the significant latent heat of fusion of silicon where the sample melts entirely, as indicated by the observation of only the broad diffuse scattering at the highest pressure achieved, 30 GPa. We demonstrate that the now conventional X-ray diffraction geometry for probing shock-compressed matter is insensitive to the onset of melting, expected in all systems at extreme conditions.

Crucially, we demonstrate a shock-induced lowering of the onset of phase transitions, and thus modification of the

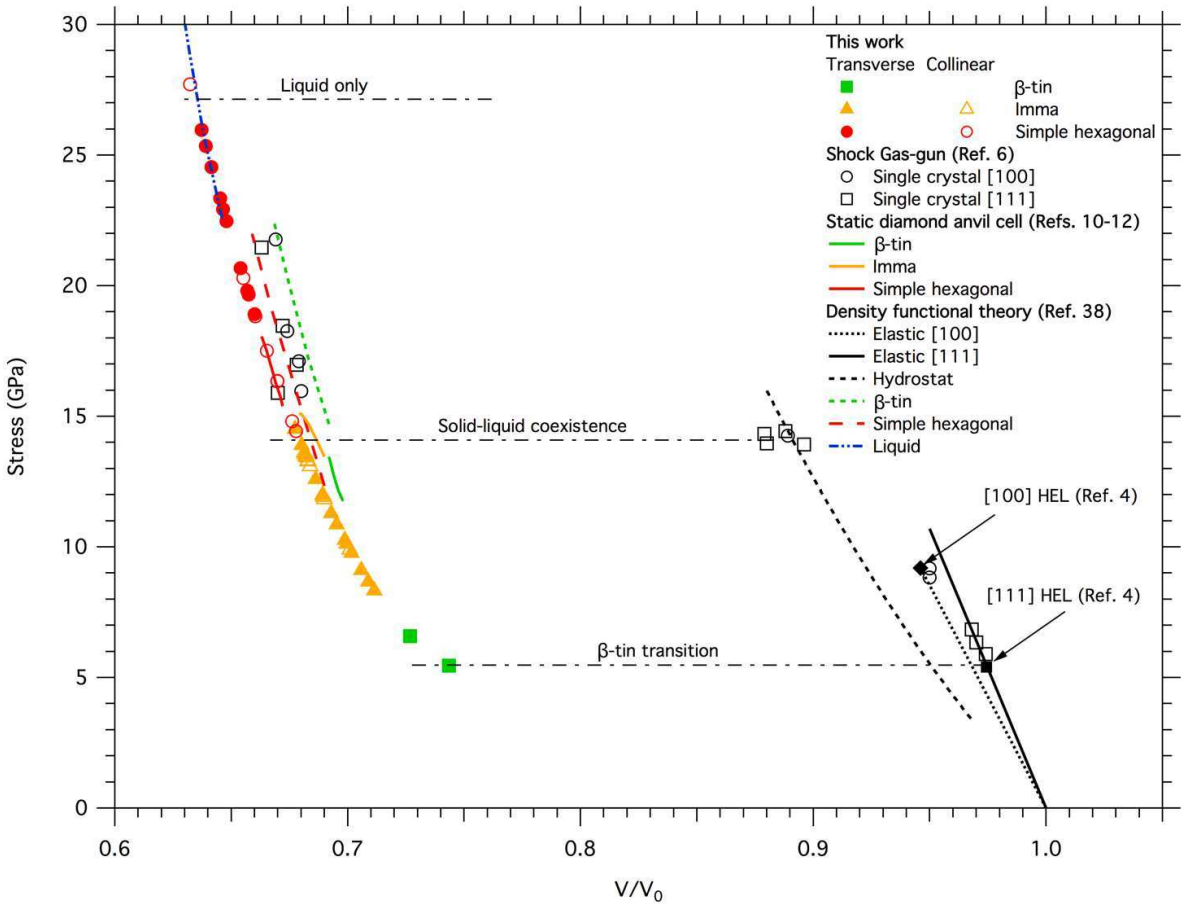

FIG. 4. **Dynamic shear-lowering of phase transition boundaries:** Stress-Volume plot of data obtained in this study, compared with density functional theory calculations (Ref. 39) and static diamond anvil cell experiments (Refs. 10-12). Hugoniot Elastic Limits for the [100] and [111] directions are from Ref. 4. Horizontal dot-dashed lines indicate phase transition boundaries from this study.

phase diagram away from that which would be determined utilising a diamond anvil cell-based (quasi-hydrostatic) approach. Here, we find the lowering of two subsequent solid-solid phase transitions: CD→ β-tin→ $Imma$, illustrating that shock-compression experiments can have a profound impact on hydrostatic phase boundaries. Previous shock-compression studies suggest that high strain-rates may cause phase transition boundaries to be shifted upwards in pressure, relative to their static boundaries[7, 8]. Clearly, the influence of shock-induced shear and strain-rate on the occurrence of phase transitions is non-trivial, and will have a significant impact when employing dynamic compression techniques to explore high pressure phases of materials found in planetary interiors, where conditions are largely hydrostatic and strain-rates are very low. In particular, careful attention will need to be paid when investigating non-metallic systems, the dominant constituents of planetary interiors, which typically exhibit higher strength, and may thus be more susceptible to the effects of shear-induced phase boundary modification.

I. ACKNOWLEDGEMENTS

E.E.M and A.S. acknowledge funding from the Volkswagen Foundation. J.S.W. is grateful for support from EPSRC under grant EP/J017256/1. This work is supported by the French Agence Nationale de la Recherche (ANR) with the ANR IRONFEL 12-PDOC-0011 Use of the Linac Coherent Light Source (LCLS), SLAC National Accelerator Laboratory, is supported by the U.S. Department of Energy, Office of Science, Office of Basic Energy Sciences under Contract No. DE-AC02-76SF00515. The MEC instrument is supported by the U.S. Department of Energy, Office of Science, Office of Fusion Energy Sciences under contract No. SF00515. The authors thank J. B. Hastings and L. B. Fletcher for a critical review of the manuscript.

II. AUTHOR CONTRIBUTIONS

E.E.M., A.H., and A.N. designed the experiment, and E.E.M., A.H., D.S. and C.S. designed the targets, and C.S. manufactured the targets. E.E.M., A.K., M.H., E.G., Z.K., H-.J.L., B.N., A.P., M.R., A.S., C.S., F.T., S.T., T.T. and A.H. contributed to the setup of the experiment and data collection. E.E.M. analysed the data, with assistance from A.K., M.H., R.F.S. and A.H.. E.E.M. and A.H. interpreted the data. E.E.M., A.H. and J.S.W. wrote the manuscript. All authors commented critically on the manuscript.

[1] Bancroft, D., Peterson, E. L. & Minshall, S., Polymorphism of iron at high pressure. *J. Appl. Phys.* **27**, 291-298 (1956)

[2] Colburn N. L., Forbes, J. W. & Jones, H. D., Electrical measurements in silicon under shock-wave compression. *J. Appl. Phys.* **43**, 5007-5012 (1972)

[3] Smith, R. F., Minich, R. W., Rudd, R. E., Eggert, J. H., Bolme, C. A., *et al.*, Orientation and rate dependence in high strain-rate compression of single-crystal silicon. *Phys. Rev. B*, **86**, 245204 (2012)

[4] Gust W. H. & Royce, E. B., Axial yield strengths and two successive phase transition stresses for crystalline silicon. *J. Appl. Phys.* **42**, 1897-1905 (1971)

[5] Goto, T., Sato, T. & Syono, Y., Reduction of shear strength and phase-transition in shock-loaded silicon. *Jpn. J. Appl. Phys* **21**, L369-L371 (1982)

[6] Turneaure, S. J., & Gupta, Y. M., Inelastic deformation and phase transformation of shock compressed silicon single crystals. *Appl. Phys. Lett.* **91**, 201913 (2007)

[7] Smith, R. F., Eggert, J. H., Saculla, M. D., Jankowski, A. F., Bastea, M., *et al.*, Ultrafast dynamic compression technique to study the kinetics of phase transformations in bismuth. *Phys. Rev. Lett.* **101**, 065701 (2008)

[8] Smith, R. F., Eggert, J. H., Swift, D. C., Wang, J., Duffy, T. S., *et al.*, Time-dependence of the alpha to epsilon phase transformation in iron. *J. Appl. Phys.* **114**, 223507 (2013)

[9] Higginbotham, A., Stubley, P. G., Comley, A. J., Eggert, J. H., Foster, J. M., *et al.*, Inelastic response of silicon to shock compression. *Sci. Rep.* **6**, 24211 (2016)

[10] Jamieson, J. C., Crystal structures at high pressures of metallic modifications of silicon and germanium, *Science* **139**, 762-764 (1963)

[11] McMahon, M. I. & Nelmes R. J., New high-pressure phase of Si. *Phys. Rev. B* **47**, 8337-8340 (1993)

[12] McMahon, M. I., Nelmes, R. J., Wright, N. G. & Allan, D. R., Pressure dependence of the Imma phase of silicon. *Phys. Rev. B* **50**, 739-743 (1994)

[13] Olijnyk, H., Sikka, S. K. & Holzapfel, W. B., Structural phase transitions in Si and Ge under pressures up to 50 GPa. *Phys. Lett. A* **103**, 137-140 (1984)

[14] Duclos, S. J., Vohra, Y. K. & Ruoff, A. L., hcp-to-fcc transition in silicon at 78 GPa and studies to 100 GPa. *Phys. Rev. Lett.* **58**, 775-777 (1987)

[15] Hanfland, M., Schwarz, U., Syassen, K. & Takemura, K., Crystal Structure of the High-Pressure Phase Silicon VI. *Phys. Rev. Lett.* **82**, 1197-1200 (1999)

[16] Wentorf, R. H., & Kasper, J. S., Two new forms of silicon. *Science* **139**, 338-339 (1963)

[17] Piltz, R. O., Maclean, J. R., Clark, S. J., Ackland, G. J., Hatton, P. D., *et al.*, Structure and properties of silicon XII: A complex tetrahedrally bonded phase. *Phys. Rev. B* **52**, 4072-4085 (1995)

[18] Mogni, G., Higginbotham, A., Gaál-Nagy, K., Park, N. & Wark, J. S., Molecular dynamics simulations of shock-compressed single-crystal silicon, *Phys. Rev. B* **89**, 064104 (2014)

[19] Nagler, B., Arnold, B., Bouchard, G., Boyce, R. F., Boyce, R. M., Callen, *et al.*, The Matter in Extreme Conditions instrument at the Linac Coherent Light Source. *J. Synchrotron Radiat.* **22**, 520-525 (2015)

[20] Fletcher, L. B., Lee, H. J., Döppner, T., Galtier, E., Nagler, B., *et al.*, Ultrabright X-ray laser scattering for dynamic warm dense matter physics. *Nature Photon.* **9**, 274-279 (2015)

[21] Gorman, M. G., Briggs, R., McBride, E. E., Higginbotham, A., Arnold, B., *et al.*, Direct observation of melting in shock-compressed bismuth with femtosecond X-ray diffraction. *Phys. Rev. Lett.* **115**, 095701 (2015)

[22] Gleason, A. E., Bolme, C. A., Lee, H. J., Nagler, B., Galtier, E., *et al.*, Ultrafast visualization of crystallization and grain growth in shock-compressed SiO_2. *Nature Comms.* **6**, 8191 (2015)

[23] Harmand, M., Ravasio, A., Mazevet, S., Bouchet, J., Denoeud, A., *et al.*, X-ray absorption spectroscopy of iron at multimegabar pressures in laser shock experiments. *Phys. Rev. B* **92**, 024108 (2015)

[24] Kraus, D., Ravasio, A., Gauthier, M., Gericke, D. O., Vorberger, J., *et al.*, Nanosecond formation of diamond and ionsdaleite by shock compression of graphite. *Nature Comms.* **7**, 10970 (2016)

[25] Rygg, J. R., Eggert, J. H., Lazicki, A. E., Coppari, F., Hawreliak, J. A., *et al.*, Powder diffraction from solids in the terapascal regime. *Rev. Sci. Inst.* **83**, 113904 (2012)

[26] Coppari, F., Smith, R. F., Eggert, J. H., Wang, J., Rygg, J. R., *et al.*, Experimental evidence for a phase transition in magnesium oxide at exoplanet pressures. *Nature Geo.* **6** 926-929 (2013)

[27] Lazicki, A., Rygg, J. R., Coppari, F., Smith, R., Fratanduono, D., *et al.*, X-ray diffraction of solid tin to 1.2 TPa. *Phys. Rev. Lett.* **115**, 075502 (2015)

[28] Wang, J., Coppari, F., Smith, R. F., Eggert, J. H., Lazicki, A. E., *et al.*, X-ray diffraction of molybdenum under shock compression to 450 GPa. *Phys. Rev. B* **92**, 174114 (2015)
[29] Le Bail, A. L., Whole powder pattern decomposition methods and applications: A retrospection. *Powder Diffraction* **20**, 316-326 (2005)
[30] Cheng, C., Huang, W. H. & Li, H. J., Thermodynamics of uniaxial phase transition: Ab initio study of the diamond-to-β-tin transition in Si and Ge. *Phys. Rev. B* **63**, 153202 (2001)
[31] Gupta, M. C. & Ruoff, A. L., Static compression of silicon in the [100] and in the [111] directions. *J. Appl. Phys.* **51**, 1072-1075 (1980)
[32] Lewis, S. P. & Cohen, M. L., Theoretical study of high-pressure orthorhombic silicon. *Phys. Rev. B* **48**, 16144-16147 (1993)
[33] Funamori, N. & Tsuji, K., Pressure-induced structural changes of liquid silicon. *Phys. Rev. Lett.* **88**, 255508 (2002)
[34] Daisenberger, D., Wilson, M., McMillan, P. F., Quesada Cabrera, R., Wilding, M. C., *et al.*, High-pressure x-ray scattering and computer simulation studies of density-induced polyamorphism in silicon. *Phys. Rev. B* **75**, 224118 (2007)
[35] Eggert, J. H., Hicks, D. G., Celliers, P. M., Bradley, D. K., McWilliams, R. S., *et al.*, Melting temperature of diamond at ultrahigh pressure. *Nature. Phys.* **6**, 40-43 (2010)
[36] Hahn, E. N., Zhao, S., Bringa, E. M. & Meyers, M. A., Supersonic dislocation bursts in silicon. *Scientific Reports* **6**, 26977 (2016)
[37] Zhao, S., Kad, B., Hahn, E. N., Remington, B. A., Wehrenberg, C. E., *et al.*, Pressure and shear-induced amorphization of silicon. *Extreme Mechanics Letters* **5**, 74 (2015)
[38] Turneaure, S. J., Sinclair, N. & Gupta, Y. M., Real-time examination of atomistic mechanisms during shock-induced structural transformation in silicon. *Phys. Rev. Lett.* **117**, 045502 (2016)
[39] Strickson, O. & Artacho, E., Ab initio calculation of the shock Hugoniot of bulk silicon. *Phys. Rev. B* **93**, 094107 (2016)
[40] Dixit, S. N., Lawson, J. K., Manes, K. R. & Powell, H. T., Kinoform phase plates for focal plane irradiance profile control. *Optics Letters* **19**, 417-419 (1994)

III. METHODS

Experimental Configuration

Experiments were conducted at the Matter in Extreme Conditions (MEC) end station at the Linear Coherent Light Source (LCLS) at SLAC National Accelerator Laboratory. Polycrystalline silicon samples were shock compressed via irradiation with both arms of the nanosecond pulsed Nd:glass laser system. The incident laser light was frequency doubled to 527 nm, and a 20 ns temporally square pulse was combined with phase plate optics producing a spatially-smoothed 250 μm spot size on target,[40] to achieve laser intensities on target in the range 2×10^{10}-2×10^{11} W/cm^2. Two experimental geometries were employed in this work: (1) A 'collinear' geometry (Supp. Info. Sec I), where the X-ray beam is incident at 11° to the target normal, and thus along the direction of shock compression, and, (2) A transverse geometry, whereby the laser beam, and hence direction of shock compression was perpendicular to the X-ray direction (Fig. 1 (a)). In both configurations, the X-ray pulse length was approximately 80 fs, and the jitter between the optical drive laser and the X-ray beam was no more than 20 ps[19].

(1) Collinear Configuration

In this configuration, velocimetry from the sample rear surface was recorded via optical velocimetry (VISAR) simultaneous with X-ray diffraction. The X-ray wavelength was 1.3051(2) Å. The beam was focussed to 40 μm, and centred on the 250 μm laser drive spot. In this configuration, X-rays were timed at 18 ns, 2 ns before the 20 ns laser pulse was turned off. This was to probe the maximum amount of material during a pressure-supported shock wave, before the falling edge of the laser pulse caused pressure to reduce. The rising edge of the pulse was measured to be 0.9 ns, and the falling edge was measured to be 2.1 ns. The same laser pulse shape was used in the transverse configuration.

(2) Transverse Configuration

The X-ray wavelength was 1.3007(5) Å and X-ray beam was focussed to 10 μm, and placed a distance of 50 μm into the silicon sample i.e. 50 μm from the ablator-silicon interface. This ensured that that the waves within the sample had separated out sufficiently to discriminate each individual wave, yet was close enough to the origin of the shock wave to ensure that wave reverberations and release from the target edges did not play a significant role. For the lowest pressures reported here, the Si targets were ablated directly. The X-ray beam was then placed 50 μm from the drive surface. The phase plates were defocussed by 2 mm to a spot size of 380 μm so that the entire target package is shock-compressed, maximising the amount of material in the shocked state. However, to reach the highest pressures, the 250 μm spot at best focus was used. Images of the laser spot, and VISAR planarity shots are found in the Supp. Info. Here, the position of the X-ray beam was placed at the same position – 50 μm – and the timing of the X-rays relative to the drive laser was varied between 14 ns and 18 ns to capture the different multiple waves traversing the target.

Target Design

Where specified, the polyimide ablators had a 100 nm coating of aluminium on both the drive surface to prevent tamped ablation. The polycrystalline silicon was quasi-single crystal in nature with grain sizes of order 100 μm. Hence, it was significantly larger than the X-ray beam in both configurations.

In the collinear configuration, targets consisted of the polyimide ablator, bonded to polycrystalline silicon, 125 μm thick in the X-ray and shock direction. Perpendicular to the shock/X-ray direction, the samples were 3×3 mm squares, significantly larger than the laser drive spot, hence limiting edge rarefaction effects at the silicon-vacuum interface. In the transverse configuration, 125 μm of polycrystalline silicon was sandwiched between two 100 μm thick silicon single crystals ([001] orientation), to provide good impedance matching and hence reduce complex wave interactions between the silicon-vacuum interface at the target edge (perpendicular to the shock direction). The polyimide ablator was bonded across all three layers of the target. Additional target information may be found in Supp. Info. Sec. II.

The transverse targets were characterised during laser-only beamtime with the VISAR diagnostic. Supp. Info. Fig. 10 a shows VISAR traces from the collinear and transverse configuration targets under identical laser conditions. For a thickness of 100 μm, there is no evidence of complex wave reverberations, and similar pressure conditions were achieved with both targets, demonstrating that at a thickness of 50 μm where we probed with the X-ray beam, one would not expect reverberations to be significant. Similarly, Supp. Info. Fig. 10 b compares diffraction from the collinear and transverse configurations, with no evidence of peak broadening, and hence pressure gradients, in the sample.

Diffraction Analysis and Interpretation

In our assignment of the high-pressure phases observed we consider that the β-tin, *Imma*, and simple hexagonal phases may all be described through a common orthorhombic cell, in which the β-tin and simple hexagonal phases are special cases of the *Imma* structure, where $a \neq b \neq c$. Here, we consider space group 74, with atoms occupying the 4(e) Wykoff positions. Using the non-standard setting where the origin is shifted to (0, -1/4, -Δ/2), one may consider the β-tin structure when $a = b \neq c$, and Δ=0.25. When $a \neq b \neq c$, $b/c = \sqrt{3}$, and $\Delta = 0.50$, one obtains the simple hexagonal structure. For the intermediate *Imma* phase, $a \neq b \neq c$, and the atomic co-ordinate Δ has a value intermediate between 0.25 and 0.50. The *Imma* phase becomes the β-tin structure when $a = b \neq c$. When $a \neq b \neq c$, $b/c = \sqrt{3}$, one obtains the simple hexagonal structure. For the intermediate *Imma* phase, $a \neq b \neq c$. All diffraction patterns discussed here were analysed both using the Le Bail method,[29] and through least-squares fitting to the observed d-spacings.

Data Availability The data that support the plots within this paper and other findings of this study are available from the corresponding author upon reasonable request